Interface stability between bare, Mn-Co spinel coated AISI 441 stainless steel and a diopside-based glass-ceramic sealant

A. G. Sabato[1], A. Chrysanthou[2], M. Salvo[1], G. Cempura[3], F. Smeacetto[1]

[1] *Department of Applied Science and Technology (DISAT), Politecnico di Torino, Italy;*

[2] *School of Engineering and Technology, University of Hertfordshire, Hatfield, UK;*

[3] *Faculty of Metals Engineering and Industrial Computer Science, AGH University of Science and Technology, Krakow, Poland;*

Abstract

This study is focused on a diopside-based glass-ceramic sealant for solid oxide fuel cells and its compatibility with AISI 441 stainless steel interconnect. The morphological and chemical stability with both bare and Mn-Co spinel coated AISI 441 steel, after 3500 h exposure at 800 °C in air, is reviewed and discussed. Post-mortem samples are morphologically and chemically analysed by SEM-EDS. Reaction products at the glass-ceramic/bare AISI 441 interface, resulting from the reaction of Mg from the sealant and Cr and Mn from the steel, are detected, without affecting negatively the integrity of the joints. In the case of Mn-Co spinel coated AISI 441, interactions between the glass-ceramic and the outer part of the Mn-Co spinel coating, along with crystallization of oxides rich in Si and Mg, are detected, but still no corrosion phenomena are present. The glass-ceramic is found to be compatible with both bare and coated AISI 441.

Keywords: Solid Oxide Cell, glass-ceramic, sealant, spinel coating, compatibility, electron microscopy.

Introduction

Solid oxide fuel cell (SOFC) technology is already a consolidated route for clean energy production, owing to the low-level of polluting or toxic products and to the flexibility of usable fuels (hydrogen, hydrocarbons, renewables and coal derived fuels). Advanced SOFC-based systems are currently being developed for both stationary and mobile power production applications [1,2].

In a SOFC system, many cells are connected to each other in a stack in order to satisfy the power density requirements. The planar stack design is, up to now, among the most common approaches, owing to its higher power output and the simplicity of manufacturing [3,4]. A critical issue in the planar stack design is the use of a sealant to prevent gas mixing. The role of the sealant is crucial in order to guarantee high stack efficiency and durability [5,6]. The sealing materials should show high gas tightness, thermo-chemical and thermo-mechanical compatibility with the coupled materials, as well as stability in the relevant operating conditions (800-900 °C, in both oxidising and reducing atmospheres) for thousands of hours [7-9].

The most widely used sealing materials have up to now been based on glass-ceramics, because of the ability to tailor their properties over a wide range of compositions and the simplicity of the sinter-crystallization process. Furthermore, they have shown superior gas tightness in comparison with other types of sealants (i.e. brazes) and higher stability in the extreme working conditions [8-10]. In these materials, the presence of a consistent residual glassy phase, after the sinter-crystallization process, can minimise the thermal stresses and provide self-healing effects, during heating/cooling cycles [7]. On the other hand, the formation of crystalline phases improves the mechanical properties and may assist in the tailoring of the thermo-mechanical behaviour [11-15].

Ba-containing glass-ceramics are among the most used sealants [8-10,15], however, during the heating, they have been reported to form the detrimental phase $BaAl_2Si_2O_8$ (celsian), which has a coefficient of thermal expansion (CTE) between $2.3 * 10^{-6} K^{-1}$ and $8 * 10^{-6} K^{-1}$ [11] which is not compatible with that of the typical joined materials ($9.5\text{-}12.5 * 10^{-6} K^{-1}$). More specifically the celsian phase $BaAl_2Si_2O_8$ presents different polymorphic forms with very different CTEs (monocelsian $2.3 * 10^{-6} K^{-1}$, exacelsian $6.6\text{-}8 * 10^{-6} K^{-1}$ and hortocelsian $4.5\text{-}7.1 * 10^{-6} K^{-1}$) [11]. As a consequence, the phase transitions could lead to high thermal stresses and sealing failure. Emerging glass-ceramics systems based on

Diopside ($CaMgSi_2O_6$) are gaining attention thanks to its high chemical stability and to the values of its CTE which lies within the desired range [15-19].

The chemical stability of the sealant should be considered not only in terms of the stability of the material itself, but also in terms of interfacial stability and chemical compatibility with the other components of the stack with which the sealant is in contact. In particular, the interfacing with Cr-containing stainless steels (typical interconnect materials) could lead to degradation reactions or to formation of unwanted phases. In the case of Ba-containing glass-ceramics, for example, some studies [8,11,15] have reported an interfacial reaction that leads to the formation of $BaCrO_4$, which has a very high CTE value (21-23 * 10^{-6} K^{-1}) at the interface with the interconnect.

Therefore, for SOFC application, it is crucial to evaluate the compatibility of the glass-ceramic sealants with the interconnect materials. From this point of view, consideration should be given to the fact that sometimes the interconnects are coated with protective layers, that are applied in order to limit the oxide scale growth and cathode Cr-poisoning [20-22]. The most widely used protective layers are Mn-Co spinel-based coatings [21,23-25]. In some stack designs, it is necessary to have an interface between the sealant and the coated interconnect. Hence, it is necessary to conduct experimental work to evaluate the compatibility and possible interaction between the sealant and the coating. Some researchers focused on this issue [19,26-29], including Chou et al. [28], who reported the degradation of the Mn-Co spinel coating when in contact with an alkaline-earth yttrium silicate sealing glass, after exposure to dual atmosphere at 800 °C for 500 h. More specifically the coating strongly reacted with the glass-ceramic.

The present study focuses on long-term tests in relevant conditions of a Diopside-based Ba-free glass-ceramic, interfaced with Mn-Co spinel coated and uncoated AISI 441 stainless steel used as interconnects. In particular, the morphological and chemical compatibility between these materials, after 3500 h exposure at 800 °C in air, has been investigated and discussed. In this work, the MnCo spinel was deposited by an electrophoretic method, while in Chou et al. [28] a slurry coating method was used to deposit the MnCo coating. The aim was to maintain the same coating formulation and to test the glass in contact with it. Since the compatibility between the seal and the MnCo based coatings is related not only to the composition of the coating, but also to its porosity and especially to the composition of the sealant, different glass-ceramic compositions could lead to different results.

The glass-ceramic studied here (labelled V9), was the subject of a previous study [30], in which it was tested in dual atmosphere for 1100 h at 800 °C, coupled with AISI 441 stainless steel. The composition of the sealant was tailored with the purpose to have suitable glass transition temperature (600 °C), sinter-crystallization behaviour suitable for obtaining a dense material and in order to obtain Diopside as main crystalline phase.

Experimental

The glass-ceramic investigated in the present study and labelled V9 has the following composition: SiO_2 50.4 wt%, Al_2O_3 8.3 wt%, MgO 13 wt%, CaO 9.3 wt%, Na_2O 10.3 wt%, B_2O_3 5.8 wt%, ZrO_2 2.9 wt%. Its production and thermal characterization has been reported elsewhere [30] along with its crystallization and sintering behaviour. It was designed using the SciGlass® database (Science Serve GmbH, SciGlass 6.6 software, Newton, MA, USA). The composition of the glass was tailored in order to have a T_g around 600°C and suitable CTE of the glass-ceramic. The optimal joining process for this system was at 850 °C for 30 min in air.

Joined “sandwich-like” samples were produced interfacing the sealant with the interconnect materials; these included bare AISI 441/V9/bare AISI 441 and Mn-Co coated AISI 441/V9/Mn-Co coated AISI 441. The sealant was deposited manually as a slurry paste in ethanol onto steel coupons which were 20 mm^2 in size.

The Mn-Co spinel protective coating was deposited on the steel coupons using electrophoretic deposition (EPD). The deposition was carried out following the procedure described in [31]. After the EPD process the coating was sintered using a two-step sintering procedure. During the first step, the coated samples were heated in Ar/H_2 (5 vol% of H_2) and during the second in static air. Both the sintering steps were carried out at 900 °C for 2 h with heating/cooling rates of 10 °C/min.

Both types of joints (with bare as well as with coated AISI 441) were characterized morphologically after the joining process in order to have a benchmark before undergoing long term aging tests.

After the joining process, the samples were subjected to a long term aging at 800 °C for 3500 h in static air. The heating up and the cooling down cycles were carried out at a rate of 5 °C/min. After the long term test the samples were prepared for morphological and chemical investigations by polishing using SiC grinding paper (grits

600/800/1000/1200/2500/4000) and subsequently with diamond suspension (MetaDi, monocrystal diamond suspension of 1 µm by Buehler, USA). The samples were then characterized by means of SEM/EDS (Merlin microscope by Zeiss). Before these analyses an Au-coating was deposited by sputtering, in order to make them electronically conductive.

The bare AISI 441/V9/bare AISI 441 sample was also studied by transmission electron microscopy and selected area electron diffraction (TEM/SAED). The lamella was prepared using Zeiss NEON CrossBeam 40 EsB. FEI Tecnai G2 and a FEI Titan (Cubed G2 60-300) microscope was used for TEM/SAED/EDS investigations on the lamella. These analyses were conducted on a thin lamella which had been sectioned using focused ion beam at the interface between the steel and the sealant.

X-ray diffraction analyses (XRD) of the aged glass-ceramic were conducted in a 2θ range between 10 ° and 70 ° and using Cu Kα radiation (PanAlytical X'Pert Pro PW3040/60, Philips). The collected spectra were identified employing X-Pert HighScore software.

Results and discussion

Both the joints (with bare and coated AISI 441) were well bonded after the joining process. The results of morphological SEM analyses, focused at the interfaces between the glass-ceramic and the steel, are reported in Fig. 1. The V9 glass-ceramic demonstrates good thermo-mechanical compatibility with bare as well as with Mn-Co spinel coated AISI 441. No cracks nor delamination were detected after the joining process suggesting a desirable thermal expansion behaviour of the interfaced materials. This is reasonable considering the CTE of the involved materials. Indeed, AISI 441 is reported to have a CTE of 11.5-12.4 [32,33] 10^{-6} K^{-1}, while Mn-Co has a CTE of 10.7-11.4 10^{-6} K^{-1} [27,32]. On the other hand, the CTE of V9 is reported to be 9.52 10^{-6} K^{-1} and 9.6 10^{-6} K^{-1} respectively after the joining process and after an aging of 1100h (both measured between 200 °C and 550 °C) [30]. The coating shows thickness around 8 µm as well as good densification and adhesion to the substrate as consequences of the sintering process.

The interface (dark area) between the $Mn_{1.5}Co_{1.5}O_4$ and the AISI substrate in fig 1b is composed by the oxide layer (Chromia and MnCrO spinel) [24,25]; its formation is due to heat treatment necessary for the densification of the $Mn_{1.5}Co_{1.5}O_4$ coating after the EPD deposition; furthermore, the joining process (at 850°C in air) also contributes to its further

development. Anyway, as demonstrated in previous works [35] the thermomechanical compatibility between the oxide layer and the $Mn_{1.5}Co_{1.5}O_4$ coating was found to be very good.

The observation of many crystals at the interface between the steel and the glass-ceramic suggests that heterogeneous nucleation has taken place at the surface of AISI 441 and of the Mn-Co spinel coating. As identified in our earlier work [30], this crystalline layer (formed during the joining process) is composed of diopside ($CaMgSi_2O_6$) which forms a barrier and prevents detrimental reactions between the Na (contained in the sealant) and the Cr from the steel. A consistent residual glassy phase is clearly visible (darker phase in the glass-ceramic). Furthermore, the interfacing with the sealant during the joining process, does not seem to affect negatively the integrity and the structure of the Mn-Co spinel protective coating, which maintained its dense and thick microstructure, that is necessary to limit Cr migration and oxidation of the steel.

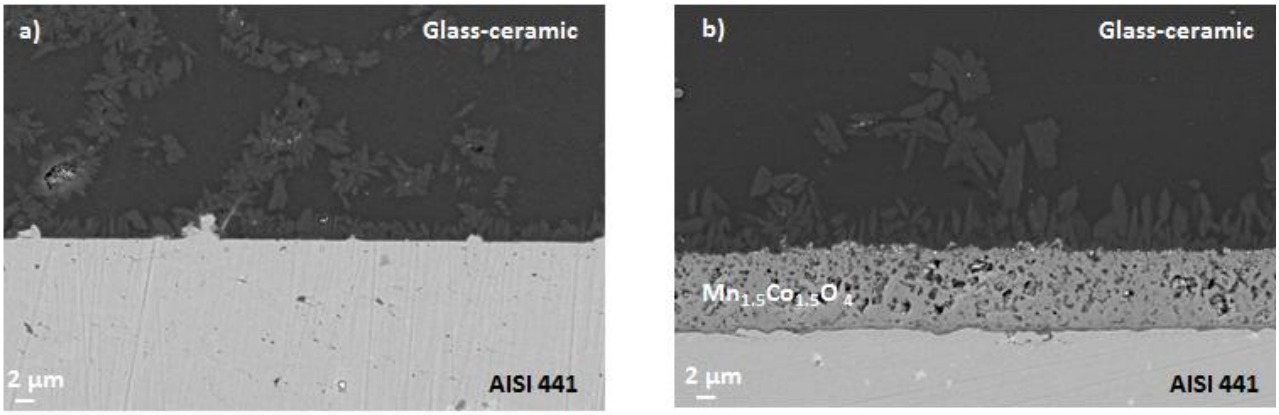

Fig. 1*: SEM images (cross section) of bare AISI 441/V9/bare AISI 441 (a) and coated AISI 441/V9/coated AISI 441 after the joining process at 850°C for 30min in air.*

The study on the V9 glass-ceramic sealant went further with the morphological and chemical analyses carried out at the interface with both bare and coated AISI 441 after aging at 800 °C for 3500 h in static air. SEM images at different magnification of the bare AISI 441/V9/bare AISI 441 sample (after the aging) are shown in Fig. 2. Fig. 2a and 2b show SEM images collected at the interface with the steel, while Fig. 2c represents part of the bulk of the glass-ceramic. The red numbers in the micrograph correspond to the position in the sample where EDS semi-quantitative analyses were undertaken and presented in Table 1. The morphological analyses provide evidence of interfacial

compatibility following long-term exposure at 800 °C; the interface is crack-free and no failure nor delamination were detected. However, the formation of new products close to the interface is visible as shown in Fig. 2a and 2b. These products grew from the oxide scale that had been formed on the surface of the steel during the aging. There is also evidence that the long term aging at 800 °C led to some microstructural changes in both the glass-ceramic and the steel. In the latter case the precipitation of bright phases is visible in the metal, while in the bulk of the glass-ceramic the precipitation of well-shaped bright crystals was detected (Fig. 2c). This phenomenon homogeneously affected the glass-ceramic (also far from the interfaces) and is present in all the investigated samples, so it is reasonable to assume that it is a characteristic of the glass-ceramic itself (its composition) and is not due to the coupling with AISI 441. Table 1 shows the composition of the bright phases in the steel (point 1) and suggests the formation of Laves phases rich in Nb, Cr, Fe and Si. The same phenomenon has been observed by Yang et al. [36] who reported the formation of $NbFe_2$ and silicides after a long period aging of AISI 441 at 800 °C in air. Silicides formation is likely to lead to a reduction in the silicon activity in the stainless steel and this will reduce the possibility of formation of an insulating silica layer at the metal/oxide scale interface. The EDS points 2 and 5 correspond to the oxide scale formed during the aging on the steel surface. The scale is coherent and well adherent to the underlying steel all along the sample. The presence of Ti and Si at these points (from the steel composition) is due to the behaviour of the AISI 441 in oxidising environments at high temperatures. Indeed, it is well known that these elements (more precisely their oxides) accumulate just under the oxide scale [36]. These are visible as darker dots in the steel side at around ≈2 μm under the oxide scale.

The compounds corresponding to points 3 and 4 in the glass-ceramic are most likely reaction products between the steel and the sealant and are composed mainly of Mg, Cr, Mn and O. These compounds seem to have grown starting from the oxide scale and complementary to it (Fig. 2b). This, together with the fact that the scale is uniformly present at the interface, suggests that the scale formed during the initial stages of the aging and subsequent reactions between Mg oxide (from the glass-ceramic, likely from the residual glassy phase) and Cr oxide (from the scale) occurred. However, the formation of these phases does not seem to have compromised the integrity of the joint and there is no evidence of cracks nor porosity at the interface. This implies good CTE agreement is maintained between these materials, even after 3500 h exposure at 800 °C in air. Concerning the glass-ceramic, the presence of crystals is visible in Fig. 2, embedded in a

residual glassy phase. This demonstrates that, despite the long aging, the amount of the glassy phase was almost unchanged; this is in agreement with previous results on the same glass-ceramic system [30]. The presence of the amorphous phase can be beneficial thanks to the possibility to provide self-healing during thermal cycling as well as thermal stress relief, above the glass-transition temperature. The composition corresponding to point 8 (crystal in the sealant) is compatible with the crystallization of diopside, already detected in the present system [30], and confirmed by the results of XRD analyses that are presented and discussed later. The same could be said for point 7, which most likely corresponds to a crystal of Albite ($NaAlSi_3O_8$). However, the longer aging in comparison with the previous study [30] has led to the precipitation of the bright crystals shown in Fig. 2c and marked as point 9. The semi-quantitative analyses, shown in Table 1 suggest that these particles are ZrO_2 which precipitated from the parent glass. Generally, this effect is used to induce heterogeneous crystallization in glass-ceramics [12]. In the present case the ZrO_2 seems to precipitate within the glassy phase and does not act as a crystallization site. Many precipitates are embedded within the amorphous matrix and appear to be isolated and no crystallization phenomena are visible starting from them. EDS point 6 was collected from the glassy phase 20 µm from the steel. No Cr has been detected in this region suggesting that no diffusion of this element from the steel/scale towards the glassy phase occurred during the aging.

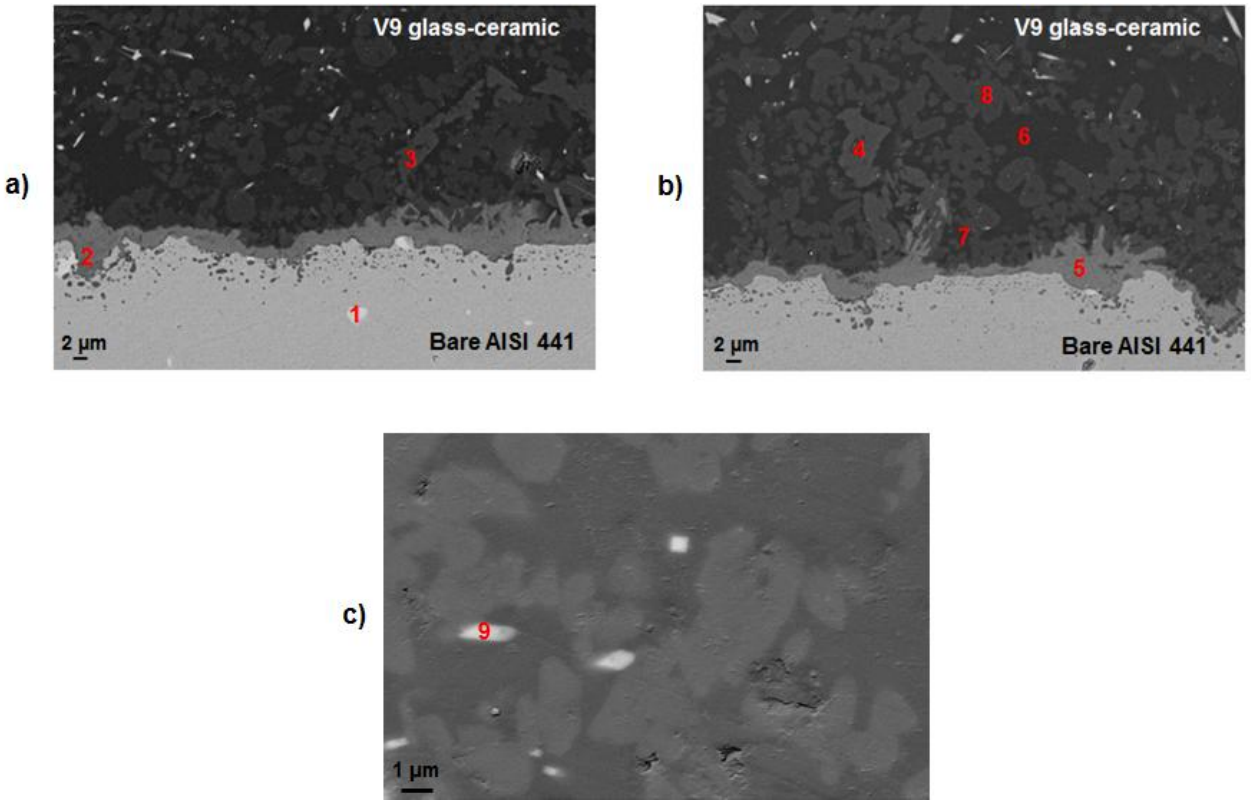

Fig. 2*: SEM images collected from the sample bare AISI 441/V9/bare AISI 441 on the interface (a, b) and in the bulk of the glass-ceramic (c), after the aging 3500 h at 800 °C in air. The red numbers correspond to the EDS semi-quantitative results reported in Table 1.*

Table 1*: EDS semi-quantitative results corresponding to the red numbers in Fig. 2.*

		EDS points								
		1	2	3	4	5	6	7	8	9
Elements (at. %)	Nb	31.7	-	-	-	-	-	-	-	-
	O	-	53	55.5	54.9	50.6	55.4	58.9	49	63.9
	Mg	-	-	23.6	23.6	1	-	2.1	11.3	-
	Cr	9.1	40.6	17.7	18.2	40.4	-	0.4	-	-
	Mn	-	1	3.2	2.7	4.5	-	-	-	-
	Fe	50.6	0.9	-	-	2.1	-	0.4	-	-
	Ti	-	1.3	-	-	0.7	-	-	-	-
	Al	-	0.8	-	0.6	-	9.1	7.8	1.6	1
	Si	8.6	2.6	-	-	0.7	27.5	22.5	26	2.2

	Ca	-	-	-	-	-	0.7	0.8	10.1	0.2
	Na	-	-	-	-	-	7.3	7.1	2	1.6
	Zr	-	-	-	-	-	-	-	-	31.1

It is interesting to note that no corrosion phenomena were detected in the sample. This is very important considering the previous study on the coupling of AISI 441/V9 [30]. In that case, strong corrosion phenomena were detected after an exposure to dual atmosphere at 800 °C for 1100 h. The absence of corrosion reported here seems to confirm that the earlier observations of corrosion [30] had indeed occurred as a consequence of exposure to the dual atmosphere and not from interaction between the sealant and the steel. This would be in agreement with other studies, in which the breakaway corrosion development is bonded to the effect of dual atmosphere exposition [37-39].

The results discussed above are concordant with the EDS elemental map reported in Fig. 3. The maps for Mn and Cr show enrichment of these metals at the interface corresponding to the formation of the oxide scale. Furthermore, in some of these regions there is evidence of the presence of Mg, confirming the formation of the reaction products discussed above and corresponding to points 3 and 4 in Table 1. The signals of Mg and Ca are both present, together with Si and O, in the crystalline phases in the glass-ceramic side and this confirms the formation of diopside.

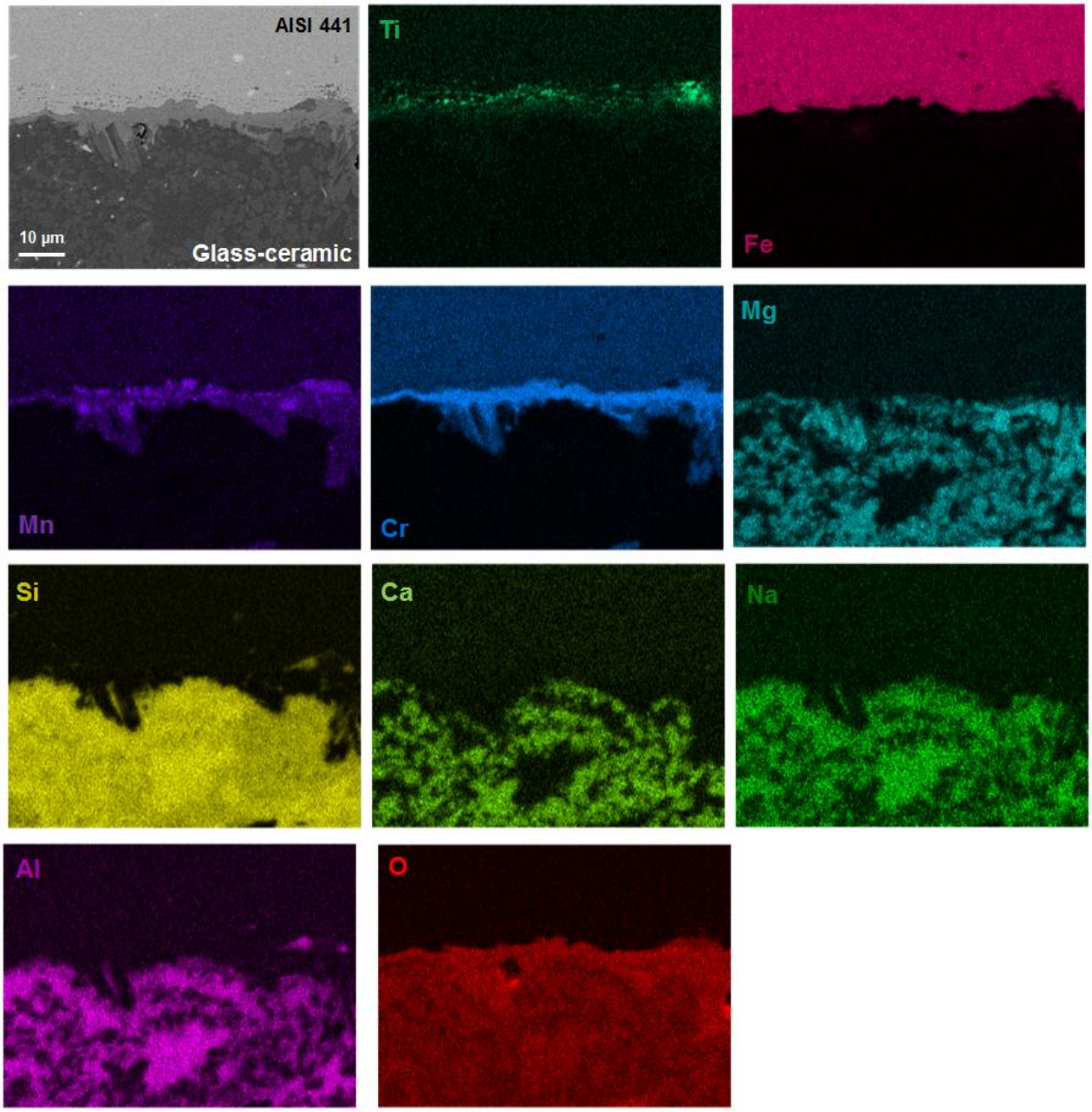

Fig. 3*: EDS elemental map collected at the interface bare AISI 441/V9 after 3500 h at 800 °C in air.*

Fig. 4 depicts the results of TEM/EDS/SAED analyses carried out on the thin lamella (obtained by focused ion beam) at the interface between bare AISI 441 and V9 glass-ceramic after the aging. The EDS maps of Cr, Mn O and Mg are in accordance with Fig. 3 showing growth of an oxide containing Mg, Cr and Mn (in minor amount) in contact with the oxide scale formed at the interface. The oxide scale thickness is around 1.5 µm coherently present in the investigated region. Three electron diffraction patterns were collected from three different regions: the oxide scale, one of the bright crystals precipitated in the glass-ceramic and the reaction product growth on the scale. The first

region was observed to be composed of Cr_2O_3 while the bright crystal was found to be ZrO_2 confirming the precipitation of this compound in the glass-ceramic as a consequence of the long aging. On the other hand, the SAED pattern collected on the reaction product seems to have the structure of $CrMn_2O_4$. It is possible that the Mg (from the glassy phase of the sealant) entered in the spinel structure of $(Cr,Mn)_3O_4$ typically formed in the outer part of the scale of chromia forming stainless steels. So this compound could be identified as a mixed spinel with a general formula $(Mg,Cr,Mn)_3O_4$. The grain of $(Mg,Cr,Mn)_3O_4$ appears to be well in contact with the underlying oxide scale as well as with the glass-ceramic sealant.

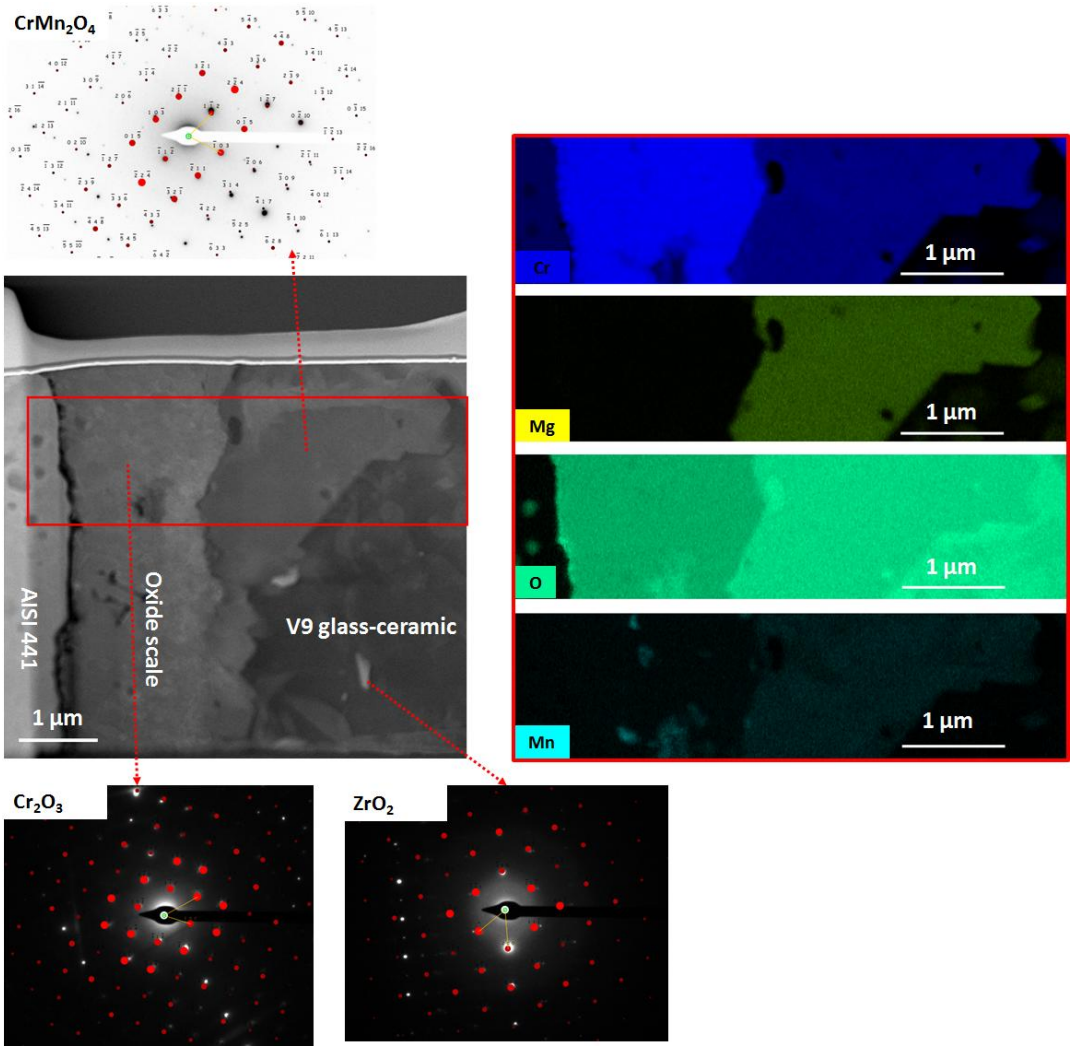

Fig. 4*: TEM/EDS/SAED analyses carried out at the interface bare AISI 441/V9 after aging at 800 °C for 3500 h in air.*

Fig. 5 depicts a SEM image collected at the interface between the Mn-Co spinel coated AISI 441 and the glass ceramic and confirms continuing compatibility between these

materials as shown in Fig. 1 following the joining process. The red numbers in Fig. 5 correspond to the points subjected to EDS analyses. The semi-quantitative EDS results are shown in Table 2. From a morphological point of view, the coating is well in contact with the underlying oxide scale, grown on the steel during aging (thickness ≈2 µm). The protective layer seems to follow well the asperities present on the surface of the steel all along the sample and shows a thickness of about ≈ 6-8 µm (after aging for 3500 h). This confirms the excellent performance in terms of thickness and homogeneity of the EPD process. Indeed, in order to act effectively as a barrier for Cr evaporation/diffusion, a good coating should be thick and dense enough. Thin coatings or coatings of low density have been demonstrated to have low Cr retention ability [20,21,35]. The absence of cracks and delamination suggests that the values of the CTE of the glass-ceramic and the steel as well as those of the protective coating and the oxide scale are suitably matched. The EDS analyses at point 1 are concordant with the composition of the oxide scale. Point 2 (collected from the middle of the coating) shows a slight presence of Cr and Fe that could be due to the volume interaction of the analysis that could collect some Cr from the region close to the interface with the scale. Indeed, some studies detected the formation of a thin (≈0.5 µm) reaction layer between the Mn-Co spinel and the Cr from the oxide scale of the steel after long term aging [35]. The presence here (very low) of Mg and Al can be due also to a slight infiltration of the glassy phase into the porosity of the coating. From the morphological point of view, the interface between the sealant and the coating seems to exhibit crystalline products. The morphology of these crystals appears different from the diopside crystals detected in the glass-ceramic, suggesting a different compound. This was confirmed by the EDS results collected at point 3 in Fig. 5. Indeed, the strong presence of Si, O and Mg was recorded here together with smaller amounts of Co and Mn. This phase is present coherently all along the interface and does not seem to negatively affect the integrity of the joining. The interactions between the protective coating and the glass-ceramic are limited to the formation of these compounds across a thickness of 2 µm above the coating. However, the integrity of the coating was maintained. This is very important, as some studies [26-28] have shown that the interaction between the sealant and the protective coating could strongly compromise the integrity of the protective layer making the application of $(MnCo)_3O_4$ on the sealing areas unsuitable. In addition, as reported by Wang et al. [29], the compatibility between the $(MnCo)_3O_4$-based coatings and the glass-ceramic can prevent detrimental reactions between the bare steel and the sealant. The sintering procedure of the coatings and the achieved density could be

another important factor. Indeed, in another previous study, the same type of coating (obtained by EPD as well but sintered only in static air) has been reported to be completely infiltrated by the glass-ceramic after aging of 500 h at 800 °C[31]. Furthermore, at point 3, no Cr was detected suggesting prevention of Cr diffusion into the glass-ceramic.

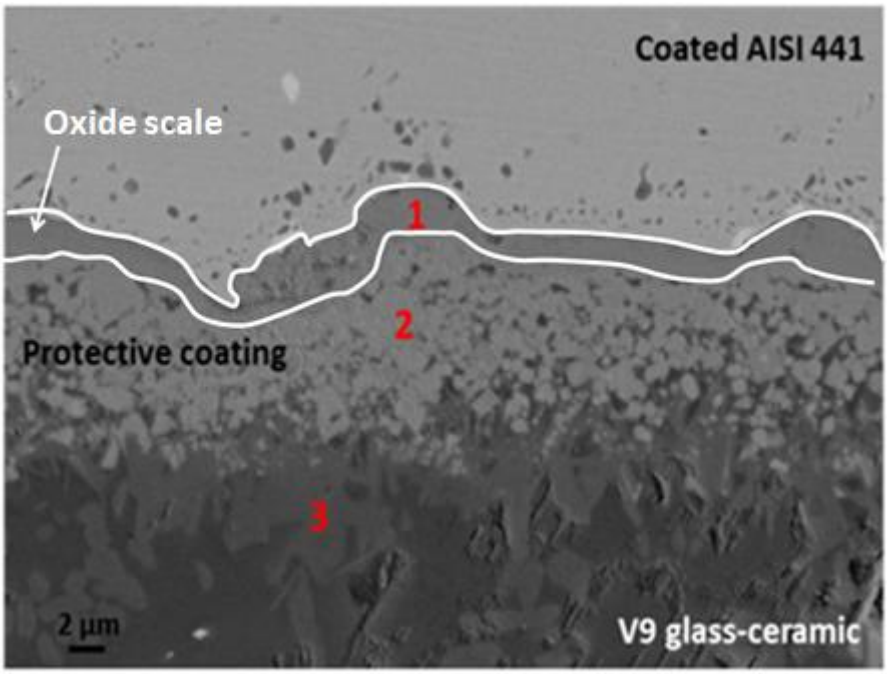

Fig. 5*: SEM image of the interface Mn-Co coated AISI 441 /V9 after 3500 h at 800 °C in air. The red numbers correspond to the point interested by EDS analyses.*

Table 2*: EDS semi-quantitative results corresponding to the red numbers in Fig. 5.*

		EDS points		
		1	2	3
Elements (at%)	O	54.2	53	53
	Ti	0.7	-	-
	Cr	34.3	3.3	-
	Mn	9.1	22.3	1.6
	Fe	1.7	0.9	-
	Mg	-	3.1	25.4
	Al	-	1	-
	Co	-	16.4	4.1
	Si	-	-	15.9

The results just discussed were further confirmed by the EDS elemental map collected at the interface and reported in Fig. 6. The map related to Cr shows that this element is situated only within the oxide scale and the steel side, confirming the ability of the Mn-Co spinel coating to prevent Cr from diffusing into the glass-ceramic. It is also possible to identify a layer just below the protective coating in which the signals for Si, O, Mg, Co and Mn (slightly) are present together. This corresponds to the crystals with composition of EDS point 3 in Table 2 and described above. From Fig. 6 the Mn seems to be present in both the oxide scale and in the coating in accordance with the results reported in Table 2. In addition, the presence of Ca, Mg, Si and O was recorded in the crystals inside the glass-ceramic. This observation is in agreement with the formation of diospide as the main crystalline phase.

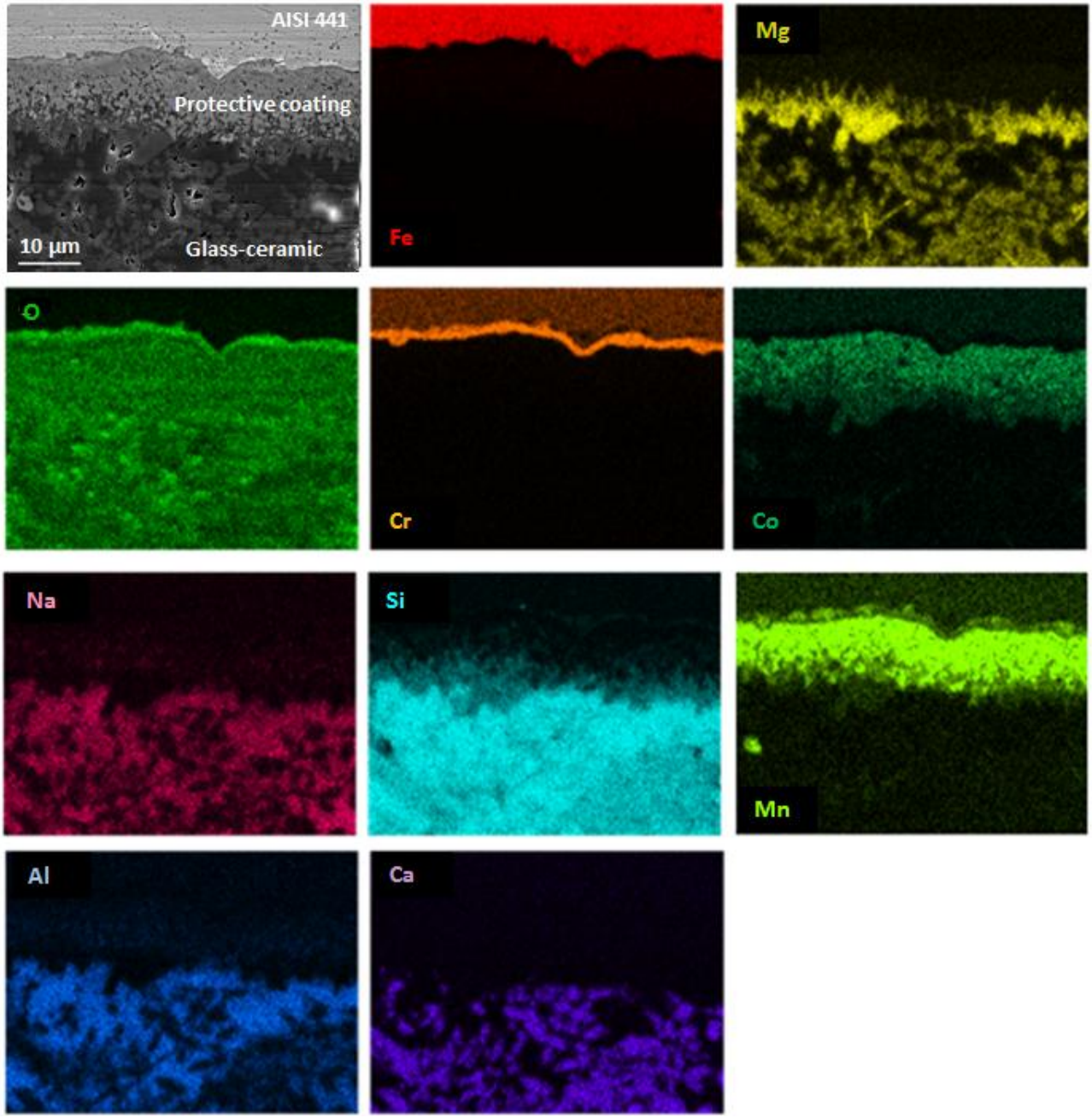

Fig. 6*: EDS elemental map collected at the interface Mn-Co coated AISI 441 /V9 after 3500 h at 800 °C in air.*

The results of the XRD analysis on V9 glass-ceramic after 3500 h at 800 °C in air are shown in Fig. 7. The crystalline phases were identified as diopside (ref. code 01-075-0945) and albite (ref. code 00-010-0393), confirming the EDS analyses. These observations are in agreement with our previous finding in [30], where these were the only detected phases after an aging of 1100 h at 800 °C. The values of CTE of these phases are well matched with the one of the overall glass-ceramic and of the joined material: 11.5 10^{-6} K^{-1} and 9 10^{-6} K^{-1}, respectively for the diopside and albite [30-34]. The diopside was formed in the glass-ceramic after the joining process. The albite was detected only after a long term aging for

1100 hrs at 800°C [30]. The strong tendency to crystallize in diopside of similar systems is well known [17,18,40]. The overall composition of the V9 parent glass was tailored not only to form diopside as the main crystalline phase, but also to tune the materials properties (such as viscosity, wettability on metal substrates) with the introduction of different oxides (such as Na_2O).

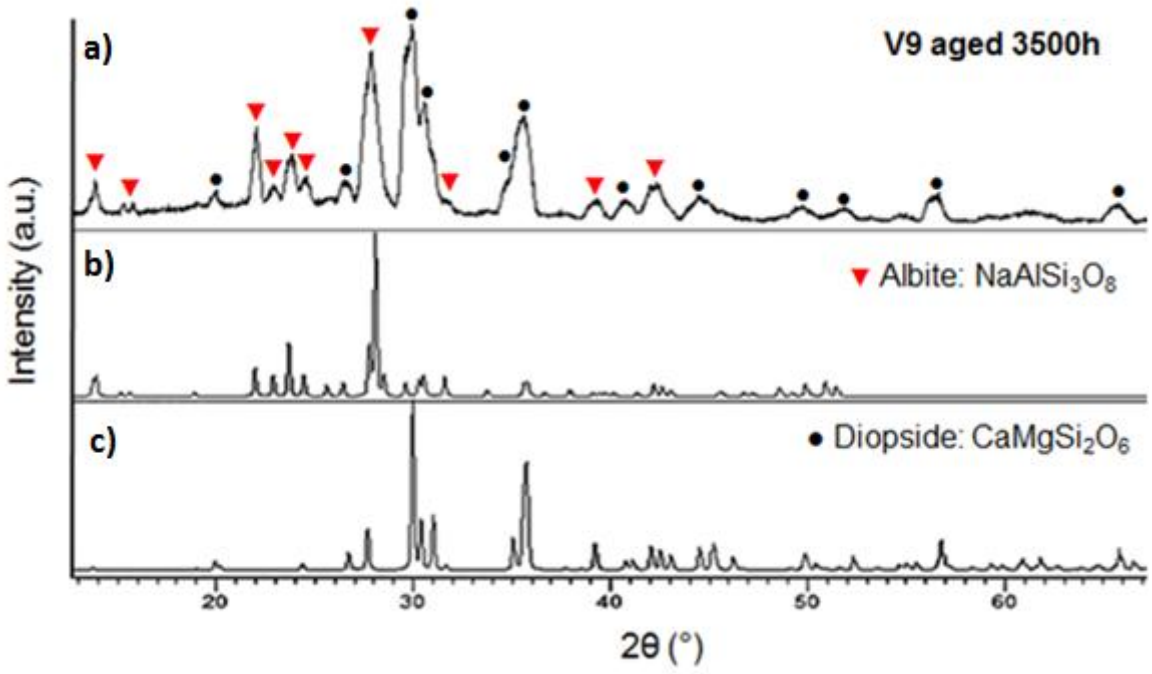

Fig. 7: *XRD pattern collected on V9 glass-ceramic after 3500 h at 800 °C in air (a), compared with simulated pattern of albite (b) and diopside (c).*

Conclusions

The present study was focused on the morphological and chemical characterization of a diopside-based glass-ceramic sealant for SOFC coupled with AISI 441 stainless steel and exposed to a 3500 h aging in air at 800 °C. The coupling with bare AISI 441 and Mn-Co spinel coated AISI 441 was very successful, because the interfaces remained intact after the joining process, as well as after the long aging to 3500 h, as a consequence of good thermo-mechanical compatibility between them. The integrity of the joints (after long exposure in relevant conditions) would ensure a hermetic seal.

No diffusion of elements from the bare AISI 441 was detected towards the sealant. However, a reaction product was detected at the interface. This resulted from the reaction of Mg from the residual glassy phase and Cr and Mn from the oxide scale. These products

grew starting from the oxide scale and complementary to it, without affecting negatively the integrity between the sealant and the steel. So no excessive CTE mismatches are expected between these products, the glass-ceramic and the oxide scale, otherwise formation of cracks would be expected starting from them. The SAED analyses revealed that the structure of these reaction products is compatible with the one of $CrMn_2O_4$. It is probable that MgO from the glassy phase dissolved into the external part of the oxide scale leading to the formation of a $(Mg,Cr,Mn)_3O_4$ spinel at the interface between the sealant and the oxide scale. This phenomenon was not detected in the previous study, indicating that this phenomenon was due to the longer exposition to 800 °C.

In the case of the Mn-Co spinel coated AISI 441, the protective coating demonstrated very good performance in its Cr-blocking ability even considering the long duration of the test. There was interaction between interfacial glass-ceramic and protective coating along with crystallization of oxides rich in Si and Mg (with traces of Mn and Co). Also in this case the growth of these species did not affect negatively the morphology of the interface.

Diopside and Albite were identified as main crystalline phases in the glass-ceramic in agreement with the authors earlier observation following aging for 1100 hrs [30].

In both of the analysed samples, no corrosion phenomena were detected. In conclusion, the glass-ceramic reported here could be considered suitable for sealing in SOFC applications when coupled with AISI 441 stainless steel or with Mn-Co spinel coated interconnects. The coating demonstrated good performance when joined with AISI 441 stainless steel and V9 glass-ceramic from the point of view of thermo-mechanical compatibility after the 3500 hrs test. The results reported here could be very important from a technological point of view. The compatibility between the sealant and the coating may suggest that the masking of the interconnect areas dedicated to the sealing, during the deposition of the protective coating, may be unnecessary. This may save a step in the production of SOFC stacks. However, this is strictly dependent on the specific stack design and for this reason it may, in any case, be important to evaluate the compatibility of the sealant with the bare steel. The present study has shown V9 glass-ceramic to be compatible with both bare and coated AISI 441.

Funding

The research leading to these results has received funding from the European Union Seventh Framework Program under Grant Agreement 312483 - ESTEEM2 (Integrated Infrastructure Initiative–I3

Captions

Fig. 1: SEM images (cross section) of bare AISI 441/V9/bare AISI 441 (a) and coated AISI 441/V9/coated AISI 441 after the joining process at 850 °C for 30 min in air.

Fig. 2: SEM images collected from the sample bare AISI 441/V9/bare AISI 441 on the interface (a, b) and in the bulk of the glass-ceramic (c), after the aging 3500 h at 800 °C in air. The red numbers correspond to the EDS semi-quantitative results reported in Table 1.

Fig. 3: EDS elemental map collected at the interface bare AISI 441/V9 after 3500 h at 800 °C in air.

Fig. 4: TEM/EDS/SAED analyses carried out at the interface bare AISI 441/V9 after aging at 800 °C for 3500 h in air.

Fig. 5: SEM image of the interface Mn-Co coated AISI 441 /V9 after 3500 h at 800 °C in air. The red numbers correspond to the point interested by EDS analyses.

Fig. 6: EDS elemental map collected at the interface Mn-Co coated AISI 441 /V9 after 3500 h at 800 °C in air.

Fig. 7: XRD pattern collected on V9 glass-ceramic after 3500 h at 800 °C in air (a), compared with simulated pattern of albite (b) and diopside (c).

Table 1: EDS semi-quantitative results corresponding to the red numbers in Fig. 2.

Table 2: EDS semi-quantitative results corresponding to the red numbers in Fig. 5.

Bibliography

[1] Sharaf OZ, Orhan MF. An overview of fuel cell technology: Fundamentals and applications. Renew Sustain Energy Rev 2014; 32: 810–53. doi:10.1016/j.rser.2014.01.012.

[2] Singhal SC. Solid oxide fuel cells for stationary, mobile, and military applications. Solid State Ionics 2002; 152–153: 405–10. doi:10.1016/S0167-2738(02)00349-1.

[3] Singhal SC, Kendall K. High-temperature solid oxide fuel cells: fundamentals, design, and applicatons. Elsevier Science; 2003.

[4] Timurkutluk B, Timurkutluk C, Mat MD, Kaplan Y. A review on cell/stack designs for high performance solid oxide fuel cells. Renew Sustain Energy Rev 2016; 56: 1101–21. doi:10.1016/j.rser.2015.12.034.

[5] Yokokawa H, Tu H, Iwanschitz B, Mai A. Fundamental mechanisms limiting solid oxide fuel cell durability. J Power Sources 2008; 182 :400–12. doi:10.1016/j.jpowsour.2008.02.016.

[6] Singh P, Minh NQ. Solid Oxide Fuel Cells: Technology Status. Int J Appl Ceram Technol 2004; 1 :5–15. doi:10.1111/j.1744-7402.2004.tb00149.x.

[7] Singh RN. Sealing Technology for Solid Oxide Fuel Cells. Int J Appl Ceram Technol 2007; 4: 134–44. doi:doi:10.1111/j.1744-7402.2007.02128.x.

[8] Mahato N, Banerjee A, Gupta A, Omar S, Balani K. Progress in material selection for solid oxide fuel cell technology: A review. Prog Mater Sci 2015; 72 :141–337. doi:10.1016/j.pmatsci.2015.01.001.

[9] Fergus JW. Sealants for solid oxide fuel cells. J Power Sources 2005; 147 :46–57. doi:10.1016/j.jpowsour.2005.05.002.

[10] Mahapatra MK, Lu K. Seal glass for solid oxide fuel cells. J Power Sources 2010; 195: 7129–39. doi:10.1016/j.jpowsour.2010.06.003.

[11] Mahapatra MK, Lu K. Glass-based seals for solid oxide fuel and electrolyzer cells - A review. Mater Sci Eng R Reports 2010; 67: 65–85. doi:10.1016/j.mser.2009.12.002.

[12] Holland W, G. Beall. Glass-ceramic technology. Westerville: The American Ceramic Society; 2002.

[13] Chang HT, Lin CK, Liu CK, Wu SH. High-temperature mechanical properties of a solid oxide fuel cell glass sealant in sintered forms. J Power Sources 2011; 196: 3583–91. doi:10.1016/j.jpowsour.2010.12.035.

[14] Chang HT, Lin CK, Liu CK. Effects of crystallization on the high-temperature mechanical properties of a glass sealant for solid oxide fuel cell. J Power Sources 2010; 195: 3159–65. doi:10.1016/j.jpowsour.2009.12.008.

[15] Tulyaganov DU, Reddy AA, Kharton V V., Ferreira JMF. Aluminosilicate-based sealants for SOFCs and other electrochemical applications - A brief review. J Power Sources 2013; 242: 486–502. doi:10.1016/j.jpowsour.2013.05.099 Review.

[16] Reddy AA, Tulyaganov DU, Pascual MJ, Kharton V V., Tsipis E V., Kolotygin VA, et al. Diopside-Ba disilicate glass-ceramic sealants for SOFCs: Enhanced adhesion and thermal stability by Sr for Ca substitution. Int J Hydrogen Energy 2013; 38: 3073–86. doi:10.1016/j.ijhydene.2012.12.074.

[17] Reddy AA, Tulyaganov DU, Goel A, Pascual MJ, Kharton V V., Tsipis E V., et al. Diopside - Mg orthosilicate and diopside - Ba disilicate glass-ceramics for sealing applications in SOFC: Sintering and chemical interactions studies. Int J Hydrogen Energy 2012; 37: 12528–39. doi:10.1016/j.ijhydene.2012.05.130.

[18] Reddy AA, Tulyaganov DU, Mather GC, Pascual MJ, Kharton V V, Bredikhin SI, et al. Effect of strontium-to-calcium ratio on the structure, crystallization behavior and functional properties of diopside-based glasses 2014; 39: 3552-3563. doi:10.1016/j.ijhydene.2013.12.104.

[19] Smeacetto F, De Miranda A, Chrysanthou A, Bernardo E, Secco M, Bindi M, et al. Novel glass-ceramic composition as sealant for SOFCs. J Am Ceram Soc 2014; 97: 3835–42. doi:10.1111/jace.13219.

[20] Mah JCW, Muchtar A, Somalu MR, Ghazali MJ. Metallic interconnects for solid oxide fuel cell: A review on protective coating and deposition techniques. Int J Hydrogen Energy 2017; 42: 9219-29. doi:10.1016/j.ijhydene.2016.03.195.

[21] Shaigan N, Qu W, Ivey DG, Chen W. A review of recent progress in coatings, surface modifications and alloy developments for solid oxide fuel cell ferritic stainless steel interconnects. J Power Sources 2010; 195: 1529–42. doi:10.1016/j.jpowsour.2009.09.069.

[22] Smeacetto F, Salvo M, Leone P, Santarelli M, Ferraris M. Performance and testing of joined Crofer22APU-glass-ceramic sealant-anode supported cell in SOFC relevant conditions. Mater Lett 2011; 65: 1048–52. doi:10.1016/j.matlet.2010.12.050.

[23] Puranen J, Laakso J, Horkanen M, Heionen S, Kilmalahti M, Lugowski S, et al. High temperature oxidation tests for the high velocity solution precursor flame sprayed manganese-cobalt oxide spinel protective coatings on SOFC interconnector steel Int J Hydrogen Energy 2015; 40: 6216-27 doi:10.1016/j.ijhydene.2015.02.129.

[24] Stevenson JW, Yang ZG, Xia GG, Nie Z, Templeton JD. Long-term oxidation behavior of spinel-coated ferritic stainless steel for solid oxide fuel cell interconnect applications. J Power Sources 2013; 231: 256–63. doi:10.1016/j.jpowsour.2013.01.033.

[25] Choi JP, Scott Weil K, Matt Chou Y, Stevenson JW, Gary Yang Z. Development of MnCoO coating with new aluminizing process for planar SOFC stacks. Int J Hydrogen Energy 2011; 36: 4549–56. doi:10.1016/j.ijhydene.2010.04.110.

[26] Mahapatra MK, Lu K. Seal glass compatibility with bare and (Mn,Co)3O4 coated Crofer 22 APU alloy in different atmospheres. J Power Sources 2011; 196: 700–8. doi:10.1016/j.jpowsour.2010.07.084.

[27] Mahapatra MK, Lu K, Liu X, Wu J. Compatibility of a seal glass with (Mn,Co)3O4 coated interconnects: Effect of atmosphere. Int J Hydrogen Energy 2010; 35: 7945–56. doi:10.1016/j.ijhydene.2010.05.070.

[28] Chou YS, Stevenson JW, Xia GG, Yang ZG. Electrical stability of a novel sealing glass with (Mn,Co)-spinel coated Crofer22APU in a simulated SOFC dual environment. J Power Sources 2010; 195: 5666–73. doi:10.1016/j.jpowsour.2010.03.052.

[29] Wang X, Ou DR, Shang L, Zhao Z, Cheng M. Sealing performance and chemical compatibility of SrO???La2O3???Al2O3???SiO2 glasses with bare and coated ferritic alloy. Ceram Int 2016; 42: 14168–74. doi:10.1016/j.ceramint.2016.06.040.

[30] Sabato AG, Cempura G, Montinaro D, Chrysanthou A, Salvo M, Bernardo E, et al. Glass-ceramic sealant for solid oxide fuel cells application: Characterization and

performance in dual atmosphere. J Power Sources 2016; 328: 262–70. doi:10.1016/j.jpowsour.2016.08.010.

[31] Smeacetto F, Miranda A De, Sandra Cabanas Polo SM, Boccaccini D, Salvo M, Boccaccini AR. Electrophoretic deposition of Mn1.5Co1.5O4 on metallic interconnect and interaction with glass-ceramic sealant for solid oxide fuel cells application. J Power Sources 2015; 280: 379–86. doi:10.1016/j.ijhydene.2013.04.106.

[32] Widgeon SJ, Corral EL, Spilde MN, Loehman RE. Glass-to-Metal Seal Interfacial Analysis using Electron Probe Microscopy for Reliable Solid Oxide Fuel Cells 2009; 786: 781–6. doi:10.1111/j.1551-2916.2008.02902.x.

[33] Technical Data Sheet ATI 441 HP. Allegheny Technologies Incorporated. 2014.

[34] Anderson OL, Isaak DG. Mineral physics and crystallography: a handbook of physical constants. Spectroscopy 1995: 357. doi:10.1029/RF002.

[35] Molin S, Sabato AG, Bindi M, Leone P, Cempura G, Salvo M, et al. Journal of the European Ceramic Society Microstructural and electrical characterization of Mn-Co spinel protective coatings for solid oxide cell interconnects. J Eur Ceram Soc 2017; 37: 4781–91. doi:10.1016/j.jeurceramsoc.2017.07.011.

[36] Yang Z, Xia G, Wang C, Nie Z, Templeton J, Stevenson JW, et al. Investigation of iron – chromium – niobium – titanium ferritic stainless steel for solid oxide fuel cell interconnect applications 2008; 183: 660–7. doi:10.1016/j.jpowsour.2008.05.037.

[37] Alnegren P, Sattari M, Svensson JE, Froitzheim J. Severe dual atmosphere effect at 600 °c for stainless steel 441. J Power Sources 2016; 301: 170–8. doi:10.1016/j.jpowsour.2015.10.001.

[38] Amendola R, Gannon P, Ellingwood B, Hoyt K, Piccardo P, Genocchio P. Oxidation behavior of coated and preoxidized ferritic steel in single and dual atmosphere exposures at 800°C. Surf Coatings Technol 2012; 206: 2173–80. doi:10.1016/j.surfcoat.2011.09.054.

[39] Ardigo MR, Popa I, Combemale L, Chevalier S, Herbst F, Girardon P. Dual atmosphere study of the K41X stainless steel for interconnect application in high temperature water vapour electrolysis. Int J Hydrogen Energy 2014; 40: 5305–12. doi:10.1016/j.ijhydene.2015.01.116.

[40] Francis AA, Rawlings RD, Sweeney R, Boccaccini AR. Crystallization kinetic of glass particles prepared from a mixture of coal ash and soda-lime cullet glass. J. non Cryst. Solids 2004; 333: 187-194. doi: 10.1016/j.jnoncrysol.2003.09.048.